Asian Journal of Physics
Vol. 31, No 2 (2022) 341-353
Available on: www.asianjournalofphysics.com

ap

Establishing the SERS-based sensing capabilities of silver nanorod thin films fabricated through oblique angle deposition at different temperatures

Adam C Stahler[1], Piyush J Shah[2*], Andrew M. Sarangan[2], and Ioana E Pavel[3*]

[1]*Electro-Optics Graduate Program, University of Dayton, 300 College Park, Dayton, OH 45469, U.S.A.*

[2]*Department of Chemistry, Wright State University, 3640 Colonel Glenn Hwy., Dayton, OH 45435, U.S.A.*

[3]*Department of Physical and Environmental Sciences,*
Texas A&M Corpus Christi, 6300 Ocean Dr, Corpus Christi, TX 78412, U.S.A.

Silver nanorod thin films (AgNRs) grown using oblique angle deposition are known to induce surface-enhanced Raman scattering (SERS) effects in analyte molecules adsorbed to their nanoscaled features. In this study, a rigorous approach was developed for comparing the SERS-based sensing capabilities of AgNR films grown at different temperatures using fluorescence emission spectroscopy (FES) in conjunction with a widely-used SERS test probe, rhodamine 6G (R6G), and scanning electron microscopy (SEM). While FES helped quantifying for the first time the number of R6G molecules adsorbed on the AgNR films, SEM measurements revealed major structural differences in the diameter, length, and tilt angle of AgNR films fabricated at cryogenic (100 K) and room temperatures (300 K). Due to the higher density (~39.5%) and increased surface area (~60.0%) of the 100 K AgNRs, significant improvements were detected in the SERS spatial performance (e.g., 100% at 10^{-7} M of R6G) and the overall intensity of the SERS signal (e.g., 445% at 10^{-7} M of R6G) in comparison with the 300 K AgNRs. The 100 K AgNRs were also found to exhibit ~10-fold larger SERS signals and enhancement factors than the widely-used Creighton, colloidal silver nanoparticles for 10^{-6} M of R6G. This novel approach for establishing SERS-based sensing capabilities could be utilized for the evaluation of a large variety of AgNR films of promising sensing applications due to their low cost and high reproducibility.

Keywords: SERS, Silver nanorod films, Oblique angle deposition, Half-mustard.

1 Introduction

Nowadays, the surface-enhanced Raman scattering (SERS) effect finds numerous cutting-edge sensing applications due to its molecular fingerprinting capabilities and low detection limits [1-4]. Single-molecule SERS detection has been reported in resonant conditions for chromophore molecules such as rhodamine 6G (R6G), which were located at the nanosized interstitial sites of aggregates of colloidal silver nanoparticles (AgNPs) [1]. These favorable locations are often referred to as hot spots. The greatly enhanced SERS signal at hot spots mainly arises due to the increase in the magnitude of the incident and the scattered electromagnetic fields associated with the excitation of coupled, localized surface plasmon resonances of AgNPs [1-4].

Among the various noble metal SERS substrates, the silver nanostructures have shown the highest enhancement factors[1-4]. Representative examples of silver SERS platforms include colloidal NPs [1-5], nanorods (NRs) manufactured at room temperature, [6-8] nanowires [9], lithographically patterned NP-arrays [10], and nano-roughened films deposited at cryogenic or room temperature [11-13]. Simple and low-cost synthetic methods are available for the colloidal AgNPs used in the single-molecule SERS experiments, but

Corresponding author
e mail: ioana.pavel@tamucc.edu (Ioana E. Pavel); *pshah1@apexmds.comedu.ar* (Piyush J. Shah)

the geometry of the hot spots generated by interacting AgNPs is difficult to control in colloidal suspensions. Additionally, fabrication techniques associated with nanowires and lithographically patterned NP-arrays are time consuming, may lead to poor SERS reproducibility and/or require the use of expensive infrastructures [9,10]. Nano-roughened silver films may overcome some of these limitations, while leading to considerable SERS enhancements. Douketis *et al* [12] and McBreen *et al* [13] showed that Ag films formed by condensation of atomic vapor onto 100 K and 300 K substrates under vacuum conditions had different SERS behaviors. The 100 K Ag films were found to lead to intense SERS spectra [12], and exhibited the largest, dipolar surface plasmon resonance for a surface roughness of approximately 350 nm [13]. High-resolution scanning tunneling microscopy revealed that the 100 K Ag films were grossly rough at the surface and had coral-like structures [12]. In contrast, the 300 K Ag films were continuous and smooth, and had poor SERS activity (i.e., no SERS spectra of good signal-to-noise ratio could be recorded for benzene and ethylene) [13]. As expected, the presence of interacting substrate features of dimensions much smaller than the wavelength of the exciting laser light (488 nm) was essential for the formation of SERS hot spots. Although the 100 K Ag films are relatively inexpensive solid substrates and have good SERS activity, they are not uniform and have large variability among the size of the coral-like nanocrystallites (i.e., a randomly rough surface) [13]. Hence, the control over the geometry of the SERS hot spots is limited (i.e., the size of the cavities between the coral-like structures).

Our previous [15] and others [6-8,14,16-19] studies have shown that oblique angle deposition (OAD) is a cost-effective and scalable method for the fabrication of highly reproducible and uniform nanostructured metallic films at room temperature (e.g., silver, titanium, chromium, and copper). Additionally, OAD offers the flexibility to change the morphological parameters of the silver nanorod (AgNR) structures such as shape, size and spatial density, which determine the geometry of the hot spots and the SERS enhancement [14,16]. Significant structural differences were observed between AgNRs that were concurrently grown at two different substrate temperatures, namely at 100 K and 300 K (i.e., the 100 K AgNRs appeared longer and thinner) [15]. It was also reported that AgNR films deposited at cryogenic temperatures exhibit improved SERS-based sensing capabilities when compared to AgNR films obtained at room temperature. However, the strategies [17-19] adopted for the evaluation of the SERS enhancement metrics of AgNR films do not accurately reflect the actual number of analyte molecules adsorbed to the nanosurface. In numerous instances [17], the morphology of the AgNR films is also assumed to be flat for the calculation of the SERS enhancement factors. The present work overcomes these limitations in the accurate characterization of the SERS-based sensing capabilities of AgNR films by using fluorescence emission spectroscopy and scanning electron microscopy (SEM). For proof of concept, AgNR films were fabricated at 100 K and 300 K, immersed in aqueous solutions of rhodamine (R6G), and allowed to dry under ambient conditions. The R6G chromophore was used as a test probe to interrogate the SERS-based sensing capabilities of the two AgNR films. Raman, SERS, SEM, and fluorescence emission measurements were then carried out on the AgNR films prior- and post-incubation with R6G at 10^{-6}, 10^{-7}, and 10^{-8} M. While SEM facilitated the characterization of the nanostructural features (e.g., the nanosurface area available for SERS binding events), the fluorescence emission spectra estimated the number of R6G molecules adsorbed on the AgNR films. To further test the SERS-based capabilities of the 100 K substrates, comparative SERS measurements were performed on the widely-used Creighton silver nanoparticles (AgNPs).

2 Experimental Methods

2.1 Oblique angle deposition (*OAD*)

In OAD, the substrate is held at an oblique angle with respect to the incoming vapor flux. As the vapor atoms condense and nucleate on the substrate, the shadowed regions behind each site stop receiving the subsequent vapor atoms. Atoms land on the previously formed droplets, resulting in the evolution of a columnar morphology.

OAD depositions were performed using an MDC evap-4000 e-beam evaporator in a generic vacuum chamber (Torr International, Inc.). The melt to substrate distance was 0.5 m. A substrate mounting plate was designed to carry liquid nitrogen (LN_2) in an open-cycle Dewar configuration.The plate had a two-piece sandwich construction with interior milled flow channels inside that were welded together and leak proofed. Copper and Teflon blocks of a preset angle of 88° were manufactured in-house and mounted side-by-side on the LN_2 carrying plate. The high and low thermal conductivities of the copper and Teflon blocks enabled the simultaneous growth of two samples under identical conditions except for the substrate temperature. Si substrates were held with a mechanical clip on the angled face of the copper and Teflon blocks. Silver paste was utilized to ensure good thermal contact between the Si substrate, the copper block, and the LN_2 carrying plate. Two type-K thermocouples were employed for the temperature measurement of the copper and Teflon blocks near the substrates. The temperature reading of the copper and Teflon blocks were approximately 100 K and 300 K, respectively, during deposition.

Prime grade Si <100> wafers were pre-cleaned with acetone, methanol, and isopropyl alcohol (IPA) before AgNR deposition. The Ag evaporation pellets had 99.99 % purity (Kurt J Lesker Company) and the chamber base pressure was less than 66.0×10^{-6} Pa (~ 0.5×1010^{-6} Torr). After the initial film conditioning ramp, the deposition rate was maintained at 0.3 nm s^{-1} for a total film thickness of 300 nm. This was achieved using a quartz crystal sensor coupled with a Sigma SQC-310 thin film deposition controller equipped with a pre-calibrated tooling factor.

2.2 Synthesis of colloidal silver nanoparticles (*AgNPs*)

Colloidal silver nanoparticles (AgNPs) were synthesized using a modified Creighton method through the reduction of silver nitrate (1 mM of $AgNO_3$, 50 mL) with sodium borohydrate aqueous solution (2 mM of $NaBH_4$, 300 mL) [5,20]. The reaction conditions and the AgNP characterization are described in previous publications [5,20,21].

2.3 Incubation of the SERS substrates with rhodamine 6G (*R6G*)

100 K and 300 K AgNR substrates (~0.5 cm× 0.5 cm) were immersed for 24 h in 2.0 mL of rhodamine 6G (R6G) at concentrations of 10^{-6} M, 10^{-7} M, and 10^{-8} M. The AgNR substrates were then removed and allowed to dry under ambient conditions before proceeding with the SERS measurements.

Creighton AgNPs (1.0 mL of colloid, 15.3 μg mL^{-1} of silver) were incubated with R6G (900 μL, 2.22×10^{-6} M) and potassium bromide (KBr, 100 μL, 1.0 M) for 24 h. This resulted in a final mixture of R6G (10^{-6} M), AgNPs (7.65 μg mL^{-1} of silver), and KBr (0.05 M). Potassium bromide (Br^- ions) was added to promote the AgNP-aggregation in the colloidal suspension and the formation of SERS hot spots through electrostatic bridges with the R6G cations [22]

2.4 Micro-Raman and surface enhanced Raman spectroscopy (*SERS*)

2.4.1 Raman system

Raman and SERS spectra were obtained using a LabRamHR 800 system (Horiba Jobin Yvon Inc.) and the associated LabSpec v.5 software. A 632.8 nm He-Ne laser was used as excitation source and the confocal hole was set at 300 μm. The backscattered Raman and SERS signals were collected using an open electrode thermo-electric cooled CCD detector (1024×526 pixels) and a 600 grooves mm^{-1} holographic grating. The laser beam spot had a diameter of about 1 μm and was focused on the samples with the help of a high resolution confocal Raman microscope (high stability BX41). Olympus objectives (100× and 50×) were employed for the data collection of samples. Under these experimental conditions, the spectral resolution was about 1 cm^{-1}.

2.4.2. Raman and SERS spectra of R6G adsorbed on Creighton AgNPs and AgNR films

Raman and SERS point spectra were obtained from the Creighton silver colloid and aqueous control samples in a 2-mL quartz cuvette. The laser power at the sample was ~15 mW. The acquisition time was 20

s and 3 s for the Raman and SERS measurements, respectively. Spectra were averaged over 10 cycles. SERS maps (50 μm×50 μm) were collected at two random locations on each AgNR film pre- and post-exposure to R6G using a step size of 5 μm. The optimized parameters were: a) 3 s acquisition time, 2 spectral cycles, and a 0.015 mW laser power at 10^{-6} M of R6G, b) 3 s, 2 cycles, and 0.15 mW at 10^{-7} M of R6G, and c) 10 s, 5 cycles, and 0.015 mW at 10^{-8} M of R6G.

Raman and SERS data analysis was conducted using MATLAB R2010b [23]. All SERS maps were normalized with respect to the integration time and the laser power. A local baseline was then subtracted from the spectral region of interest (1625 – 1675 cm^{-1}) and the integrated peak area of the xanthene breathing mode **21** of R6G at 1650 cm^{-1} was calculated. SERS images of the AgNR substrates exposed to varying R6G concentrations were constructed from the integrated area values of the xanthene peak for each pixel spectrum.

All spectra in the two SERS maps collected on the same film piece at 10^{-6} M and 10^{-7} M were averaged (n = 200). Five spectra exhibiting good signal-to-noise ratios and all characteristic modes of R6G were also averaged for the SERS maps of the 100 K and 300 K AgNRs immersed in 10^{-8} M of R6G. At this concentration, a smaller number of pixels was found to be SERS-active due to the lower amount of R6G molecules that were available for adsorption. The average SERS spectra were then baseline corrected in OriginPro 8 and the integrated area of the xanthene breathing mode was determined for all R6G concentrations. These values were subsequently used to estimate the enhancement factors of the SERS substrates.

2.5 Fluorescence emission spectrophotometry

The fluorescence emission spectra of all R6G solutions were collected in a quartz cuvette using a Cary Eclipse fluorescence spectrophotometer (Agilent Technologies, Inc.). The pre-scan option was engaged to optimize the acquisition parameters. The excitation wavelength was 530 nm and the emission spectra were collected in the 545-700 nm range using PMT detector voltages of 540, 680, and 900 V for the R6G aqueous solutions of 10^{-6}, 10^{-7}, and 10^{-8} M, respectively. The scan rate was 600 nm min^{-1}. 100 K and 300 K AgNR films of varying dimensions (n = 6) were immersed in 2 mL of each R6G aqueous solution and removed after 24 h. Fluorescence emission spectra were also obtained from the remaining R6G solutions post-exposure to the AgNR films through immersion into the R6G aqueous solutions. After the removal of the SERS substrates, optical images, which were acquired with the confocal Raman microscope, facilitated the determination of the planar surface area of the film pieces. This value was then used for the calculation of the total nanostructured surface available for R6G binding (Table S1, Supporting Information).

The percent of R6G molecules adsorbed on the AgNR substrates was estimated by calculating the percent difference in the fluorescence emission intensity of the R6G peak at 551 nm pre- and post-exposures of the AgNR thin films according to the following equation [5,21].

$$\% = \text{R6G Adsorbed molecules} = \frac{\text{Intensity}_{\text{pre-exposure}} - \text{Intensity}_{\text{post-exposure}}}{\text{Intensity}_{\text{pre-exposure}}} \times 100\% \quad (1)$$

2.6 Scanning electron microscopy (*SEM*)

SEM images of the nanostructured thin films were acquired using a Hitachi S-4800 high resolution SEM with cross-sectional and top views. Image J software was used to estimate the density and size of AgNRs (i.e., length, diameter, and nanostructured surface area) [24]. All rods within 1 μm^2 area were counted from the top view SEM images (n = 3). The length and diameter of the AgNRs were determined from the SEM cross-sectional images (n = 4). The inclination angle of the AgNRs relative to the silicon substrate was measured similarly as the length and diameter (n = 4).

3 Results and Discussion

Figure 1 shows the top and cross section SEM images of 100 K and 300 K AgNR films prior- and post-exposure into R6G aqueous solutions, respectively. Morphological differences were observed between the two AgNR samples due to the reduction in surface diffusion and the mobility of adsorbed atoms on the substrate surface [15]. Nanostructural differences were quantified in Image J software by analyzing AgNRs from the SEM images (n = 4 setions of 1 μm^2 area each). The 100 K AgNRs had a thinner diameter (28%) and were longer (56%) than those grown at 300 K (Table 1). As a result, the 100 K films had a higher density of AgNRs (~39.5%) and a larger surface area (~60.0 %) than the 300 K films (Table 1). This is an important result as the magnitude of the SERS enhancement and the spatial performance of the SERS platforms are greatly influenced by these structural features, in particular by the increase in surface area for the 100 K AgNRs.

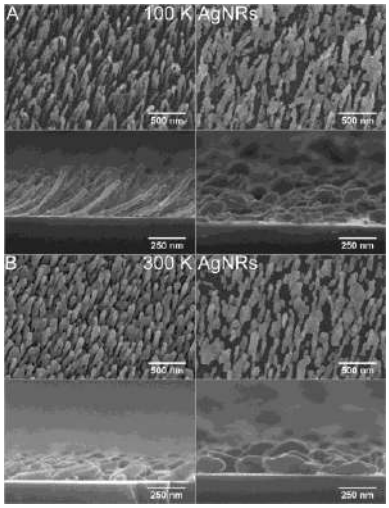

Fig 1. AgNR thin films fabricated at (A) 100 K and (B) 300 K. Top view and cross section SEM images of the AgNR films (Left) prior- and (Right) post-exposure to 10^{-6} M of R6G aqueous solution.

Table 1. Differences in the structural features of the 100 K and 300 K AgNR thin films as estimated from SEM data[a]

AgNRs	100 K	300 K
Length (nm)	428 ± 20	273 ± 21
Diameter (nm)	36 ± 10	50 ± 3
Tilt angle (°)	41.4 ± 9.7	18.8 ± 1.8
Density (# μm^{-2})	53 ± 5	38 ± 4
S.A. (m^2 μm^{-2})	2.72 ± 0.08×10^{-12}	1.70 ± 0.24×10^{-12}

[a]Tilt angle - angle relative to silicon substrate, Density - number of individual NRs per μm^2, S.A. - total nanosurface area.

Figure 2 shows the SERS images that were collected from 50 μm×50 μm random areas on the 100 K and 300 K AgNR films, after incubation with R6G at 10^{-6}, 10^{-7}, and 10^{-8} M. Similar SERS results were obtained on a second set of AgNR samples (Figs S1 and S2, Supporting Information). The SERS images were color coded according to the integrated area values. White and red pixels (5 μm pixel size) in the SERS images correspond to large integrated area values of the xanthene band (i.e., extremely active SERS regions), while dark blue and black pixels are indicative of very small or zero integrated area values of the same peak

(i.e., regions of minimum or no SERS activity). For quantitative and qualitative comparisons, all SERS maps in Fig 2 were normalized with respect to the largest integrated area value within the maps, the acquisition time, and the laser power.

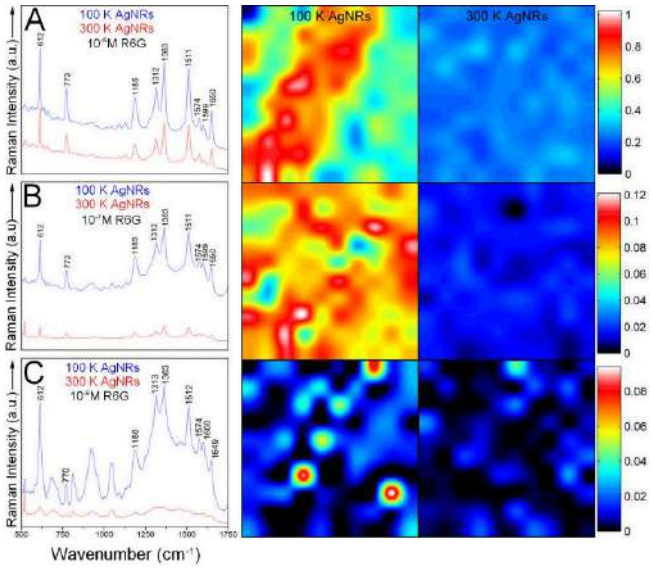

Fig 2. (Left column) Average SERS spectra obtained from the adjacent maps. SERS maps constructed from the integrated area of the xanthene breathing mode (1625-1675 cm^{-1}) of R6G molecules adsorbed on the 100 K AgNRs (Center column) and 300 K AgNRs (Right column). Rows A, B, and C designate AgNRs immersed in R6G at 10^{-6}, 10^{-7}, and 10^{-8} M, respectively.

The qualitative examination of the normalized maps shows that the 100 K AgNR films have significantly improved SERS-based sensing capabilities when compared to the 300 K AgNR films at all R6G concentrations (Fig 2). It is remarkable that all map pixels were SERS-active at 10^{-6} and 10^{-7} M of R6G for both 100 K and 300 K AgNR films. However, the cryogenic platform exhibited a percent spatial improvement in SERS signal of 95% and 100% at 10^{-6} M and 10^{-7} M of R6G, respectively, when compared to the room temperature film (Fig 3A). These percent values were estimated by determining the number of SERS pixels in the 100 K AgNR map that possessed a greater integrated area than the maximum integrated area in the 300 K AgNR map. Approximately, 71% and 68% of the total pixels were SERS-active at 10^{-8} M of R6G in the 100 K and 300 K AgNR maps, respectively. At this analyte concentration, the percent spatial improvement was determined to be 5% (Fig 3A). This smaller percent value of spatial improvement is probably due to the trace amounts of R6G molecules that are available for AgNR binding at 10^{-8} M. As the SERS maps showed, the R6G molecules were sparsely adsorbed on the surface of the 100 K AgNR films at this concentration. In fact, sub-monolayer coverage with R6G molecules was determined at 10^{-8} M for both the 100 K (0.22-fold the monolayer coverage) and the 300 K AgNR films (0.37-fold the monolayer coverage). The percent layer coverage on the 100 K and 300 K AgNR films was determined from the number of R6G molecules adsorbed onto AgNRs at each concentration (from fluorescence emission results as described below), the binding surface area of R6G (222.0 $Å^2$), and the total nanostructured surface area of the AgNRs (Table S1, Supporting Information). The binding surface area of a R6G molecule was reported to be 222.0 Å [2] by Gupta and Weimer based on semi-empirical calculations [25].

To quantify the overall percent increase in signal for the cryogenic substrate, the SERS-active pixels of each map were averaged in MatLab. The average SERS spectra are shown in Fig 2 for each R6G

concentration. The 100 K AgNR films were found to lead to an average signal enhancement of approximately 91%, 445% and 411 % when compared to the 300 K AgNRs films at 10^{-6}, 10^{-7}, and 10^{-8} M of R6G, respectively. The smaller increase in signal at 10^{-6} M (91 %) may be justified by the nanosurface saturation with R6G at 10^{-6} M (~11- and 17-fold the monolayer coverage on the 100 K and 300 K AgNR films, respectively).

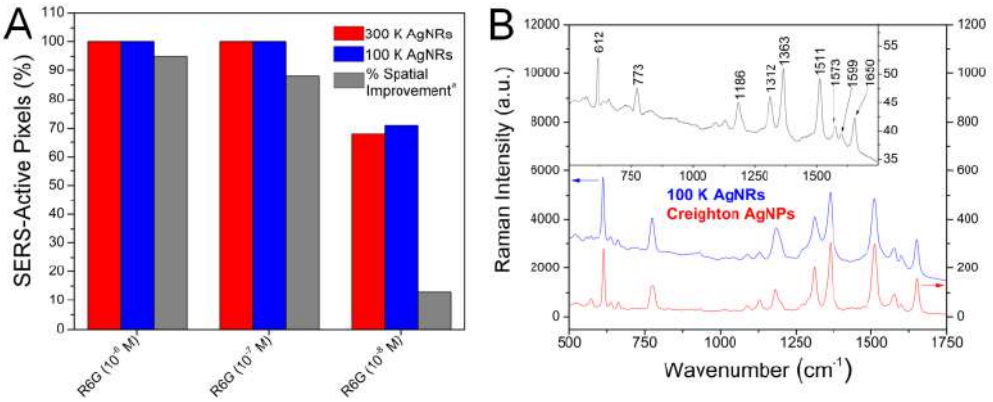

Fig 3. (A) Percent of SERS-active pixels within each map and percent spatial improvement in SERS signal. (B) Comparison between the SERS spectra obtained on 100 K AgNRs and Creighton colloidal AgNPs, incubated with R6G aqueous solution (10^{-6} M). Inset displays the control Raman spectrum of R6G aqueous solution (10^{-3} M).

The fluorescence emission measurements facilitated the accurate determination of the surface enhancement factors (SEFs) by estimating the number of R6G molecules adsorbed on the AgNR films and actually contributing to the signal enhancement. The decrease in relative intensity of the R6G emission peak at 551 nm (Fig S3, Supporting Information) was due to the inability of R6G molecules to fluoresce because of their adsorption on the AgNR surface [21,22]. It was found that a high percent of R6G molecules were adsorbed on AgNRs (e.g., 84 ± 9% of R6G molecules at 10^{-8} M). This value was scaled to the area of the laser spot and was used in the calculation of the SERS enhancement factor:

$$\mathrm{SEF} = \frac{\mathrm{Int\ Area_{SERS}}}{\mathrm{Int\ Area_{Raman}}} \times \frac{\mathrm{N_{Vol}}}{\mathrm{N_{Surf}}} \tag{2}$$

where N_{Vol} is the number of R6G molecules in the focal volume for the ordinary Raman measurement (1.14×10^7) and N_{Surf} is the number of R6G molecules adsorbed on the SERS substrate and excited by the laser beam (Table S1, Supporting Information). The baseline corrected integrated area values of the xanthene marker band (1625 cm^{-1} – 1675 cm^{-1}) were determined from the Raman spectrum of the R6G aqueous solution (Int. $Area_{Raman}$ at 10^{-3} M) and the average SERS spectra of R6G (Int.$Area_{SERS}$ at 10^{-6}, 10^{-7}, and 10^{-8} M) after normalizing with respect to the laser power and the acquisition time. The focal volume (FV ~1.896×10^{-17} m^3) was estimated using the numerical aperture of the objective (N.A.), and the excitation wavelength (λ):[25]

$$\mathrm{FV} = \pi \times \left(\frac{1.22 \times \lambda}{2 \times \mathrm{N.A.}}\right)^2 \times \left(\frac{4 \times \lambda}{\mathrm{N.A.}^2}\right) \tag{3}$$

The first term gives the waist diameter (0.965 µm) of the laser spot size, while the second term represents the depth of focus (~ 10 µm). Thus, the number of R6G molecules (N_{Vol}) present in the focal volume during the Raman measurement of the aqueous solution at 10^{-3} M was 1.14×10^7.

SEFs for 100 K AgNRs were estimated to be 5.0×10^2, 3.2×10^2, and 6.0×10^3 at R6G concentrations of 10^{-6}, 10^{-7}, and 10^{-8} M, respectively. The corresponding SEFs for 300 K AgNRs were 2.8×10^2, 1.4×10^2,

and 1.1×10^3, respectively. If the concentration difference is considered, the SERS enhancements of 100 K AgNRs (SEF ~ 2.7×10^5) approach those of truncated, colloidal silver nanoprisms (SEF = 3.2×105) at 4.5 × 10^{-9} M of R6G. These nanoprisms are one of the best resonators in SERS [22]. We offer several explanations for the significant improvement in the SERS signal for the 100 K AgNRs when compared to the 300 K AgNRs. It was hypothesized that the higher density and larger surface area of the 100 K AgNRs would accommodate a greater number of R6G molecules on the SERS substrate, under the laser beam. An additional contribution to the signal enhancement for R6G solutions is associated with the permanent collapse of the AgNR structures as a result of aqueous exposure and ambient drying. It is known that NR thin films exposed to liquids undergo permanent, structural changes (e.g., Ag and SiO_2) [26,27]. Both AgNR films appeared uniform prior exposure but had a different morphology during the acquisition of the post-exposure SERS spectra (Fig 1). The 100 K AgNRs were more severely damaged than the 300 K AgNRs probably due to their fragile nature. The 100 K AgNRs are much thinner and longer than the 300 K AgNRs, and possess a steeper angle with respect to the silicon substrate (Table 1). As a result, the mechanical spring constant of individual 100 K AgNRs is much smaller compared to that of 300 K AgNRs. Therefore, capillary forces associated with the high surface tension of water more easily damaged the AgNRs fabricated at cryogenic temperatures. The SEM images illustrated the random collapse of the 100 K AgNRs post-exposure (Fig 1). Numerous 100 K AgNRs were bundled together as a result of the structural damage and/or the aggregation promoted by the R6G analyte. Top view SEM images showed that the 100 K film was entirely covered with AgNRs prior to the immersion. However, exposed silicon areas were detected post-immersion in all substrates. The 100 K AgNRs had a greater polydispersity in size and shape than the 300 K AgNRs post-immersion. These factors may have also contributed to the large SERS enhancement that was observed post-immersion for the bundled 100 K AgNRs (i.e., the formation of hot spots). The 300 K AgNRs appeared semi-collapsed prior to incubation but better withstood the capillary forces due to the much thicker diameter, shorter lengths and more acute angle with respect to the silicon holder. The estimated shallow angle of the 300 K AgNRs confirmed this observation (18.8 ± 1.8º pre-immersion and 15.8 ± 6.4º post-immersion).

The Creighton synthesis is a common fabrication method for aqueous colloids of moderately polydispersed AgNPs (diameters of 1-140 nm) through the reduction of silver nitrate with sodium borohydride [5,20,21]. It is widely-used in numerous SERS applications because of its low cost and simplicity. In this study, the SERS-based sensing capability of 100 K AgNR films was compared to that of Creighton AgNPs (15.3 μg mL^{-1} of silver, average diameter of 10.4 nm) [21] using the newly developed evaluation approach. Colloidal AgNPs were incubated with R6G aqueous solution for 24 hours (10^{-6} M) and the SERS spectra were collected in a quartz cuvette similarly to the 100 K AgNRs. Potassium bromide (5.0×10^{-2} M) was added to the colloidal mixture to promote the AgNP-aggregation and the formation of SERS hot spots through electrostatic bridges with the R6G cations. The presence of potassium bromide had no significant influence on the generation of SERS spectra from AgNRs. The average SERS signal obtained on the 100 K AgNRs was found to be ~10-fold stronger than the one collected from AgNPs (Fig 3B). This led to a ~10-fold improvement in the SEF value of the 100 K AgNPs (5.0×10^2) when compared to the Creighton AgNPs (5.1×10^1)[21] at 10^{-6} M of R6G. Our previous SERS studies [21] on Creighton colloids also indicated that only ~70% of the R6G molecules were captured by AgNPs and contributed to the signal enhancement. In contrast, all map pixels of the 100 K AgNR films were SERS-active at 10^{-6} of R6G and a nanosurface saturation with R6G molecules was achieved (~11-fold the monolayer coverage). Nevertheless, AgNPs and AgNRs have their own advantages and disadvantages. Colloidal AgNPs are one of the "cleanest" SERS substrates, for which air exposure and contamination may be minimized or eliminated. On the other hand, AgNR films may be easily contaminated during ambient exposure. In fact, a few vibrational modes associated with organic impurities (e.g., 813, 920, 1002, and 1040 cm^{-1}) were detected in the SERS spectra from AgNRs at 10^{-8} M of R6G.

4 Conclusions

A novel approach for establishing the SERS-based sensing capabilities of AgNR films was successfully developed and tested on uniform AgNR thin films, which were grown at 100 K and 300 K using a scalable and low cost OAD technique. To accurately estimate the SERS enhancement metrics: (a) FES measurements were carried out for the first time, for the quantification of the number of R6G molecules adsorbed on the AgNR films, and (b) SEM images were collected to demonstrate the expected, major structural differences in the diameter, length, and tilt angle of AgNR films. Thereby, the 100 K AgNR films were found to possess significantly improved SERS-based sensing capabilities when compared to the widely-used Creighton colloidal AgNPs and the 300 K AgNR films. This was attributed to the higher density, increased surface area, and greater polydispersity of the 100 K AgNR films post-exposure to aqueous analytes. The SERS substrates fabricated at cryogenic temperatures are robust, lead to reproducible SERS results, and may find diverse sensing applications. The proposed approach could be utilized for the evaluation of the SERS-based sensing capabilities of a large variety of AgNR films of promising sensing applications.

Supporting Information

The spectral data obtained on duplicate AgNR films are provided in this section. This material is available free of charge.

Author Contributions

All authors have given approval to the final version of the manuscript.

Acknowledgement

I.P.S. acknowledges the Texas A&M -Corpus Christi and Wright State University support.

Abbreviations

AgNPs, silver nanoparticles; AgNRs, silver nanorods; SERS, surface-enhanced Raman spectroscopy/scattering; OAD, oblique angle deposition; R6G, rhodamine 6G.

References

1. Nie S, Emory S R, Probing single molecules and single nanoparticles by surface-enhanced Raman scattering, *Science*, 275(1997)1102–1106.
2. Xu S, Ju X, Xu W, Li X, Wang L, Bai Y, Zhao B, Ozaki Y, Immunoassay using probe-labelling immunogold nanoparticles with silver staining enhancement via surface-enhanced Raman scattering, *Analyst*, 129(2004)63–68.
3. Kneipp K, Wang Y, Kneipp H, Perelman L T, Itzkan I, Dasari R R, Feld M S, Single molecule detection using surface-enhanced Raman scattering (SERS), *Phys Rev Lett*, 78(1997)1667–1670.
4. Pavel I, McCarney E, Elkhaled A, Morrill A, Plaxco K, Moskovits M S, Label-free SERS detection of small proteins modified to act as bifunctional linkers, *J Phys Chem C*, 112(2008)4880–4883.
5. Pavel I, Alnajjar K, Monahan J, Stahler A, Hunter N, Weaver K, Baker J, Meyerhoefer A, Dolson D J, Estimating the Analytical and Surface Enhancement Factors in Surface-Enhanced Raman Scattering (SERS): A Novel Physical Chemistry and Nanotechnology Laboratory Experiment, *Chem Educ*, 89(2012)286–290.
6. Driskell J, Shanmukh S, Liu Y, Chaney S, Tang X.-J, Zhao Y.-P, Dluhy R, The use of aligned silver nanorod arrays prepared by oblique angle deposition as surface enhanced Raman scattering substrates, *J Phys Chem C*, 112(2008)895–901.
7. Driskell J, Shanmukh S, Liu Y, Hennigan S, Jones L, Zhao Y, Dluhy R, Krause D, Tripp R, Infectious agent detection with SERS-active silver nanorod arrays prepared by oblique angle deposition, *IEEE Sensors J*, 8(2008)863–870.
8. Chu H, Huang Y, Zhao Y, Silver nanorod arrays as a surface-enhanced Raman scattering substrate for foodborne pathogenic bacteria detection, *Appl Spectrosc*, 62(2008)922–931.

9. Wu Y, Livneh T, Zhang Y, Cheng G, Wang J, Tang J, Moskovits M, Stucky G, *Nano Lett*, 4(2004)2337–2342.
10. Felidj N, Aubard J, Levi G, Krenn J, Hohenau A, Schider G, Leitner A, Aussenegg F, Optimized surface-enhanced Raman scattering on gold nanoparticle arrays, *Appl Phys Lett*, 82(2003)3095; doi.org/10.1063/1.1571979.
11. Schlegel V, Cotton T, Silver-island films as substrates for enhanced Raman scattering: effect of deposition rate on intensity, *Anal Chem*, 63(1991)241–247.
12. Douketis C, Wang Z, Haslett T L, Moskovits M, Fractal character of cold-deposited silver films determined by low-temperature scanning tunneling microscopy, *Phys Rev B*, 51(1995)11022–11032.
13. McBreen P H, Moskovits M, Optical properties of silver films deposited at low temperatures, *J Appl Phys*, 54(1983)329–335.
14. Liu Y, Chu H, Zhao Y, Silver nanorod array substrates fabricated by oblique angle deposition: morphological, optical, and SERS characterizations, *J Phys Chem C*, 114(2010)8176–8183.
15. Benson M, Shah P, Marciniak M, Sarangan A, Urbas A, Optical characterization of silver nanorod thin films grown using oblique angle deposition, *J Nanomater*, 2014(2014); doi.org/10.1155/2014/694982.
16. Hawkeye M, Brett M, Glancing angle deposition: Fabrication, properties, and applications of micro-and nanostructured thin films, *J Vac Sci Technol A*, 25(2007)1317; doi.org/10.1116/1.2764082-1335.
17. Oh M.-K, Shin Y.-S, Lee C.-L, De R, Kang H, Yu N E, Kim B H, Kim J H, Morphological and SERS properties of silver nanorod array films fabricated by oblique thermal evaporation at various substrate temperatures, *Nanoscale Res Lett*, 10(2015)259; doi.org/10.1186/s11671-015-0962-8.
18. Lee J, Min K, Kim Y, Yu H K, Surface-enhanced Raman spectroscopy (SERS) study using oblique angle deposition of Ag using different substrates, *Materials*, 12(2019)1581; doi.org/10.3390/ma12101581.
19. Hui D, Zhou S, Cai C, Song S, Wu Z, Song J, Zhang Da, Meng X, Lu Bo, Duan Y, Tursun H, Gibson D, Plasma Enhanced Fluorine-Free Superhydrophobic Polyester (PET) Fabric with Ultra-Robust Antibacterial and Antibacterial Adhesion Properties, *Coatings*, 11(2021)1–15.
20. Creighton J A, Blatchford C G, Albrecht M G, Plasma resonance enhancement of Raman scattering by pyridine adsorbed on silver or gold sol particles of size comparable to the excitation wavelength, *J Chem Soc*, *Faraday Trans*, 2(1979)790–798.
21. Trefry J C, Monahan J L, Weaver K M, Meyerhoefer A J, Markopolous M M, Arnold Z S, Wooley D P, Pavel I E, Size selection and concentration of silver nanoparticles by tangential flow ultrafiltration for SERS-based biosensors, *J Am Chem Soc*, 132(2010)10970–10972.
22. Ciou S H, Cao Y W, Huang H.-C, Su D Y, Huang C L, SERS enhancement factors studies of silver nanoprism and spherical nanoparticle colloids in the presence of bromide ions, *J Phys Chem C*, 113(2009)9520–9525.
23. The Mathworks, Inc, Natick, MA, USA.
24. Abramoff M D, Magalhaes P J, Ram S J, Image processing with ImageJ, *Biophotonics Int*, 11(2004)36–42.
25. Pavel I, McCarney E, Elkhaled A, Morrill A, Plaxco K, Moskovits M, Label-free SERS detection of small proteins modified to act as bifunctional linkers, *J Phys Chem C*, 112(2008)4880–4883.
26. Shah P, Ju D, Niu X, Sarangan A M, Vapor phase sensing using metal nanorod thin films grown by cryogenic oblique angle deposition, *J Sens*, (2013), 823041; doi.org/10.1155/2013/823041.
27. Fan J, Dyer D, Zhang G, Zhoa Y, Nanocarpet effect: pattern formation during the wetting of vertically aligned nanorod arrays, *Nano Lett*, 4(2004)2133–2138.

[Received: 24.12.2021; accepted: 26.01.2022]

Supporting Information

Establishing the SERS-based sensing capabilities of silver nanorod thin films fabricated through oblique angle deposition at different temperatures

Adam C Stahler[1], Piyush J Shah[2],* Andrew M Sarangan[2], and Ioana E Pavel[3]*

Second set of SERS maps

Duplicate SERS maps were collected from AgNR substrates fabricated at a different dates, and SERS images were constructed following the procedure described in the Experimental section of the manuscript. Analysis revealed that the duplicate 100 K AgNR film also possessed improved SERS-based sensing capabilities when compared to the 300 K AgNR film (Figs S1 and S2). The average SERS spectra are shown in Fig S2 for each R6G concentration. The 100 K AgNR film was found to lead to an average signal enhancement of approximately 13%, 100% and 544% with respect to the 300 K AgNRs film at 10^{-6}, 10^{-7}, and 10^{-8} M of R6G, respectively. All pixels were SERS-active in both AgNR films at R6G concentrations of 10^{-6} and 10^{-7} M (Fig S1). The percent of SERS-active pixels at 10^{-8} M was calculated to be 76 % and 42 % for the 100 K and 300 K AgNR films, respectively. The percent spatial improvement for this second set of SERS maps was 61%, 88%, and 13% at 10^{-6}, 10^{-7}, and 10^{-8} M of R6G, respectively.

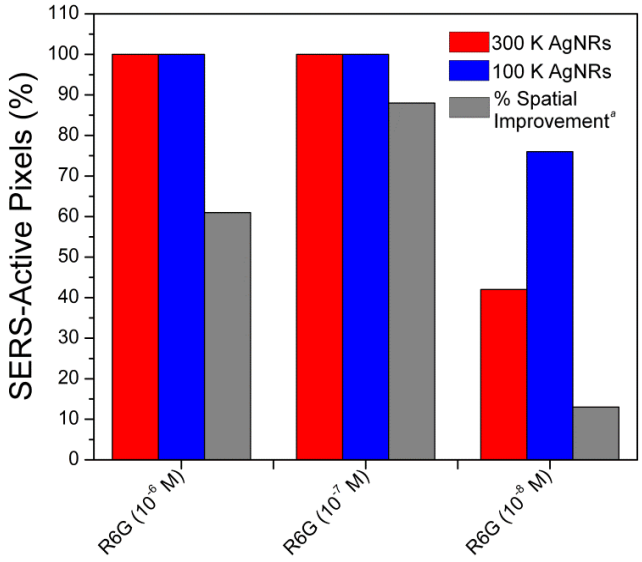

Fig S1: Percent of SERS-active pixels within each map and percent spatial improvement in SERS signal for each duplicate sample.

Fluorescence emission spectra

Figure S3 (Left) shows the fluorescence spectra of 10^{-6} M of R6G prior- and post-exposure to the 100 K AgNR films of three different dimensions. A near linear increase (R^2 = 0.9401) was observed for the percent R6G molecules adsorbed on the AgNR films with the increase in the total nanostructured surface area (Fig S3, Right). The fluorescence emission peak allowed for the estimation of the percent R6G molecules adsorbed onto AgNRs at each concentration. This methodology was repeated for all R6G concentrations. The second set of AgNR samples exhibited a larger degree of contamination (i.e., nanosites not available for R6G binding) than the first set and resulted in larger deviations from linearity at 10^{-7} and 10^{-8} M of R6G.

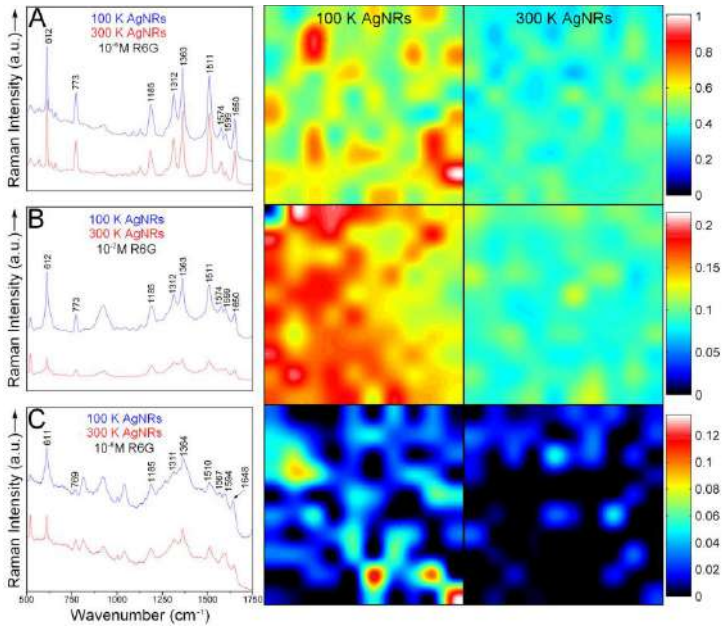

Fig S2: (Left column) Average SERS spectra obtained from the adjacent maps. SERS maps constructed from the integrated area of the xanthene breathing mode (1625-1675 cm^{-1}) of R6G molecules adsorbed on the 100 K AgNR (Center column) and (Right Column) 300 K AgNR (Right column) duplicate samples. Rows A, B, and C designate AgNRs immersed in R6G at 10^{-6}, 10^{-7}, and 10^{-8} M, respectively.

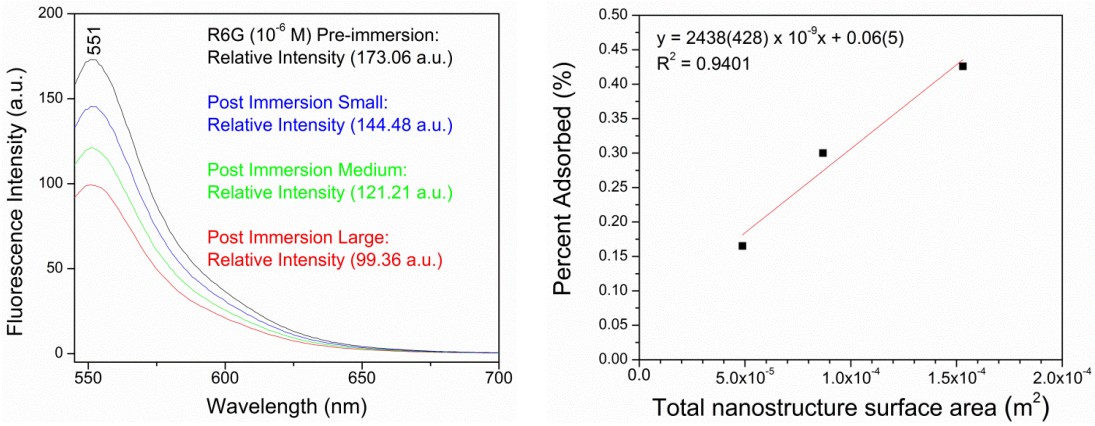

Fig S3: (Left) Fluorescence emission spectra of R6G aqueous solution (10^{-6} M) prior- and post-exposure to the 100 K AgNR substrates of three different dimensions (denoted small, medium and large). (Right) Percent R6G molecules adsorbed onto the 100 K AgNR films versus the total nanostructured surface area of each substrate.

Therefore, the % absorbance values were averaged (Table S1). However, statistical analysis revealed no significant difference between the percentage of R6G molecules adsorbed on the 100 K versus 300 K AgNR substrates as detected via one-way ANOVA ($P \leq 0.001$) and Holm-Sidak multiple comparison tests ($P \leq 0.05$).

SEF factors of duplicate SERS maps

The SEF values of the duplicate samples were similar to those obtained for the first set of samples at 10^{-6} and 10^{-7} M of R6G (> monolayer coverage). It should be noted that some differences in the SEF values were noticed at 10^{-8} M of R6G (< monolayer coverage) depending on the SERS geometry and the number of hot spots available within the sections (50 µm×50 µm area), which were randomly selected for SERS analysis. The SEFs of the 100 K AgNRs and 300 K AgNRs immersed in 10^{-6} M R6G were 8.1×10^{2} and 6.9×10^{2}, respectively. The SEFs (3.6×10^{2}) of the two substrates were identical at 10^{-7} M of R6G. This is probably due to the fact that this 100 K AgNR film sample was ~45% smaller than the 300 K AgNRs sample, and resulted in a smaller total nanostructured surface area (i.e., a much larger number of R6G molecules under the laser beam). The SEFs of the 100 K and 300 K AgNRs immersed in 10^{-8} M R6G were determined to be 3.6×10^{3} and 1.3×10^{3}, respectively.

Table S1: Average surface area of AgNR film pieces, percent of R6G molecules adsorbed onto these substrates, and number of R6G molecules within the excitation area (n = 6).

R6G Concentration (M)	AgNR Film	Surface Area (m^2)	Adsorption (%)	Number of Molecules within Excitation Spot
1×10^{-6}	100 K AgNRs	$(1.0 \pm 0.5)\times10^{-4}$	29 ± 9	$(6.7 \pm 3.9)\times10^{6}$
	300 K AgNRs	$(6.0 \pm 3.0)\times10^{-5}$	25 ± 13	$(6.3 \pm 4.5)\times10^{6}$
1×10^{-7}	100 K AgNRs	$(1.0 \pm 0.5)\times10^{-4}$	45 ± 18	$(1.0 \pm 0.7)\times10^{6}$
	300 K AgNRs	$(6.0 \pm 4.0)\times10^{-5}$	41 ± 20	$(1.0 \pm 0.9)\times10^{6}$
1×10^{-8}	100 K AgNRs	$(9.0 \pm 3.0)\times10^{-5}$	84 ± 9	$(2.2 \pm 0.5)\times10^{5}$
	300 K AgNRs	$(6.0 \pm 3.0)\times10^{-5}$	73 ± 18	$(4.4 \pm 2.4)\times10^{4}$